The 2017 World Congress on
Advances in Structural Engineering and Mechanics (ASEM17)
28 August - 1 September, 2017, Ilsan(Seoul), Korea

Development of a FRP-Wrapped Spiral Corrugated Tube for Seismic Performance of Reinforced Concrete Columns

*Chung-Che Chou[1)], Chung-Sheng Lee[2)], Kai-Yi Wu[3)] and V-Liam Chin[4)]

[1), 3), 4)] *Department of Civil Engineering, National Taiwan University, Taiwan*
[2)] *National Science and Technology Center for Disaster Reduction, Taiwan*
[1)] *cechou@ntu.edu.tw*

ABSTRACT

This paper presents a work for the development of a new fiber reinforced polymer (FRP) tube for seismic application. A proposed column consists of a FRP-Wrapped Spiral Corrugated Tube (FWSCT) filled with concrete. Five specimens were cyclically tested to investigate the flexural and shear strengths of FWSCT columns under different axial load ratios and number of FRP layers. Five specimens named as FWSCT series used only longitudinal reinforcement to provide flexural capacity and did not use transverse steel hoops in the entire column. Test results showed that Specimen FWSCT-0 experienced shear failure at about 1% drift; Specimen FWSCT-1 experienced flexural-shear failure at about 4% drift. Specimens FWSCT-3, FWSCT-5 and FWSCT-8 exhibited rupture of longitudinal reinforcement from 7% to 8% drift. A plastic hinge was formed at the top and bottom column end, extending into the footing. An analytical method that used a residual shear model and a measured plastic hinge length reasonably predicts the flexural and shear capacities of the FWSCT columns in tests.

1. INTRODUCTION

Fiber-reinforced polymer (FRP) material has shown large application in civil engineering, especially for retrofitting reinforced concrete columns or beams (Priestly and Seible 1991; Xiao et al. 1996). The light weight, high strength or stiffness-to-weight ratio, good corrosion resistance, easy handling and installation are also making FRP widely adopted in new structural members (Teng et al. 2007; Gould and Harmon 2002). Seible et al. (1996) developed a composite shell system (CSS) that contains screw threads in the inner wall to act as a shear connector between a FRP shell and concrete, transferring axial forces from concrete to the shell. The appearance of longitudinal and

---

[1)] Professor

[2)] Associate Research Fellow

[3) 4)] Graduate Student Researcher

transverse inner ribs in the FRP tube helps to distribute confining pressure and arrest growth of concrete cracks in the shell (Mirmiran et al. 1998). However, the application of FRP ribs increases the difficulty in the fabrication of a FRP tube. A new hybrid confinement tube, FRP-wrapped spiral corrugated tube (FWSCT), was proposed in this work to simplify the fabrication of a ribbed surface between concrete and FRP in a tube (Chou et al. 2014).

2. FRP-WRAPPED SPIRAL CORRUGATED TUBE (FWSCT)

A FRP-wrapped spiral corrugated tube (FWSCT) is made with a spiral corrugated steel tube wrapped by FRP (Figure 1). The spiral corrugated tube is used as an inner form for the fabrication of a FRP jacket; screw threads of the spiral corrugated tube considerably decrease the difficulty of manufacturing FRP ribs. The inner ribs of the spiral corrugated tube provide bonding mechanism between concrete and FRP, maintaining the cross sectional integrity. The FWSCT provides not only confinement but also a shear-resisting mechanism to concrete columns.

2.1 *Confined concrete model*

A dilatancy-based confined concrete model of Lee and Hegemier (2009) was used to predict the flexural and shear behaviors of FWSCT columns. A perfect bonding between the spiral corrugated tube and concrete is assumed for strain compatibility, and the geometry of spiral corrugated tube is simplified to be a pseudo flat tube. The confining stress, f_l, to concrete is considered as the summation of confining pressures provided by the spiral corrugated tube, $f_{l,s}$, and the FRP jacket, $f_{l,frp}$, which are expressed as

$$f_{l,s} = \frac{2\varepsilon_l \times E_s \times t_s}{D'} \;;\quad f_{l,frp} = \frac{2\varepsilon_l \times E_f \times t_f}{D'} \tag{1}$$

where D' is the interior diameter of the spiral corrugated tube; E_s is the elastic modulus of the spiral corrugated tube; t_s is the pseudo thickness of the assumed flat tube; E_f is the elastic modulus of the FRP jacket in hoop direction; t_f is the thickness of the FRP jacket; ε_l is the lateral strain of concrete, function of concrete compression strain (Pantazopolou and Mills 1995; Lee and Hegemier 2009).

The confinement effectiveness f_{cc}/f_c and the axial strain ε_{cc} of confined concrete at any level of lateral strain ε_l are expressed as

$$\frac{f_{cc}}{f_c} = 1 + 3.75\left(\frac{f_l}{f_c}\right)^{0.83} \tag{2}$$

$$E_{\sec(i)} = \frac{f_c}{\varepsilon_c} = \frac{f_{cc}}{\varepsilon_{cc}} \tag{3}$$

where f_{cc} and f_c are the axial stress of confined and unconfined concrete at the same lateral strain ε_l, and E_{sec} is the axial secant stiffness, which is function of lateral strain ε_l.

2.2 *Flexural behavior*

A strip analysis of the cross section is adopted to calculate the force displacement relationship of specimens. Four materials are included in the moment-curvature

analysis: confined concrete, longitudinal reinforcement, spiral corrugated tube and FRP. An interactive procedure is used to calculate the neutral axis of the cross section and associated strain under a specified curvature.

The displacement of specimens in the post-yield stage is

$$\Delta = \frac{M}{M_y}\Delta_y + \phi_p L_p\left(L_{eff} - L_p\right) \tag{4}$$

where M_y and Δ_y are the idealized moment and displacement, respectively; M is the moment corresponding to the plastic curvature ϕ_p; L_{eff} is the effective column length (Priestley et al. 1996). The plastic hinge length of the FWSCT column is composed of a "gap" and the yield-penetration length of longitudinal reinforcement inside the footing, where the "gap" is defined as the length without wrapping GFRP on the column end (Wu 2015).The ultimate displacement Δ_u of the specimen is determined based on the following: (1) the extreme concrete fiber reaches the ultimate compression strain when the FRP jacket ruptures or (2) the longitudinal reinforcement reaches 60% of the ultimate tensile strain.

2.3 *Shear behavior*

The residual shear strength model (Lee 2006) are used to calculate shear strength of FWSCT columns. This model considers the dilation of inner concrete in the compression zone, which reduce the shear capacity of the FWSCT. The nominal shear strength V_n of FWSCT columns is expressed as

$$V_n = V_c + V_p + R_{frp}V_{frp} + R_{sct}V_{sct} \tag{5}$$

$$V_c = \alpha_c\beta_c\gamma_c\sqrt{f_c'}\left(0.8A_g\right) \tag{6}$$

where V_c is the concrete resistance of aggregate interlock; V_p is the horizontal component of the applied axial load through arch action (Kowalsky and Priestly 2000). The factor α_c accounts for the column aspect ratio; the factor β_c depends on the longitudinal steel ratio; the factor γ_c represents the shear strength reduction due to an increase of displacement ductility. Since shear strengths of the FRP jacket and the spiral corrugated tube are reduced due to dilatation of concrete, parameters R_{frp} and R_{sct} are proposed to consider shear reduction for the FRP jacket strength, V_{frp}, and the spiral corrugated tube strength, V_{sct}, respectively:

$$V_{frp} = \frac{\pi}{2}t_f E_f \varepsilon_{fe}(D-c)cot\theta \;\; ; \quad V_{sct} = \frac{\pi}{2}t_s f_{y,sct}(D-c)cot\theta \tag{7}$$

$$R_{frp} = \left(1 - \frac{\varepsilon_l}{\varepsilon_{fe}}\right) \;\; ; \quad R_{sct} = \left(1 - \frac{\varepsilon_l}{\varepsilon_{su,j}}\right) \tag{8}$$

where θ is the angle between the vertical axis and shear crack; c is the depth of the neutral axis; $\varepsilon_{fe}(=0.5\varepsilon_{fu})$ is the effective strain of FRP jacket; $\varepsilon_{su,j}$ is the ultimate strain in steel jacket, taken as 60% of the rupture strain from coupon tests (Lee 2006), and $f_{y,sct}$ is the yield strength of the spiral corrugated tube.

3. EXPERIMENTAL PROGRAM

3.1 *Specimens*

Five circular concrete column specimens were designed and tested in this work (Table 1 and Figure 2(a)). The height and diameter of specimens were 2000 mm and 600 mm, respectively. Five circular concrete specimens that had no transverse reinforcement along the entire column were confined by a spiral corrugated steel tube and zero, one, three, five and eight GFRP layers, respectively. A total of 12 No.8 longitudinal reinforcement was used in each specimen. Specimens FWSCT-0, FWSCT-1 and FWSCT-3 were designed to experience shear failure based on ACI 440 (2008), with the nominal shear strength of 622 kN, 715 kN and 905 kN, respectively (Chin 2016). Specimens FWSCT-5 and FWSCT-8 were aimed to study the flexural behavior of FWSCT columns under different axial load ratio. Specimen FWSCT-8 is subjected to a high axial load ratio ($0.65P_n$) and others are subjected to a low axial load ratio ($\approx 0.2P_n$). The nominal axial capacity, P_n, considers the axial strength of unconfined concrete core and longitudinal reinforcement:

Columns were cast vertically from a single batch of concrete, specified to be 35 MPa. Table 1 shows material properties of longitudinal reinforcement and concrete cylinders at the day of test. A unidirectional GFRP (L900-E) was used to fabricate the FWSCT, where the matrix was composed of Eternal vinyl ester resin (Bisphenol A) and ETERSET 2960PT-S. The longitudinal elastic modulus and the ultimate strain of GFRP coupons were 26 to 28 GPa and 0.019 to 0.025, respectively. The spiral corrugated tube was SPCC steel with a measured elastic modulus of 163 GPa and a yield strength of 330 MPa.

3.2 *Testing*

The experiments were conducted by using a Multi-Axial Testing System, MATS (Figure 2(b)). Five FWSCT circular columns were tested using double-curvature bending, with an increasing cyclic displacement and a constant axial load. The test was stopped when the specimen was unable to maintain the applied axial load or its strength decreased below 70% of the maximum lateral force.

4. TEST RESULTS

4.1 *Test observation*

Specimen FWSCT-0 experienced shear failure at 1.4% drift due to inadequate shear strength. Figure 3(a) shows a big diagonal shear crack across through the spiral corrugated tube and concrete; the angle between the crack and the vertical axis is 25 degree. Figure 4(a) shows the load-displacement relationship of Specimen FWSCT-0 with a maximum lateral force of 911 kN.

Specimen FWSCT-1 failed at 4% drift, resulting in ductile shear failure of the column. Dashed line in Figure 4(b) shows the force-displacement relationship of Specimen FWSCT-1. The lateral strength degraded below 80% of the peak lateral force after 4% drift. The test was stopped at 6% drift after losing most of the lateral strength. Delamination of GFRP jacket was observed at the bottom part of column (Figure 3(b)). Premature failure of GFRP was caused by the imperfection of fiber

orientation in some parts; the measured maximum strain was about 0.9% (0.36ε_{fu}) at 4% drift.

Specimen FWSCT-3 failed at 7% drift (ductility of 10.4) due to fracture of longitudinal reinforcement. Unlike Specimens FWSCT-0 and FWSCT-1 without sufficient shear strength, no diagonal shear crack or fiber rupture were found throughout the test. Figure 4(b) shows the comparison of force-displacement relationship between Specimens FWSCT-1 and FWSCT-3. Specimen FWSCT-3 had a complete flexural response, indicating that three GFRP layers provide sufficient shear resistance and confinement to concrete core. Specimens FWSCT-5 and FWSCT-8 had similar responses (Figure 4(c) and (d)), which exhibited fracture of longitudinal reinforcement at 7% and 8% drifts, respectively. Concrete flexural cracks that were found at the top and bottom unwrapped column-to-footing regions also penetrated into the footing after 3% drift. For Specimen FWSCT-8 under a constant high axial load (0.65P_n=6856 kN), no buckling of longitudinal reinforcement occurred throughout the test, indicating that the FWSCT can provide sufficient confinement and shear resistance to columns under a high axial load and large drift (Figure 3(c)).

4.2 *Overall Comparison*

Table 2 lists test results of Specimens FWSCT-0, FWSCT-1, FWSCT-3, FWSCT-5 and FWSCT-8. Concrete columns with the GFRP-wrapped spiral corrugated tube show good lateral strength and deformation capability. Shear failure of Specimen FWSCT-0 at a ductility of 1.12 is prevented by wrapping one GFRP layer to Specimen FWSCT-1 that reaches a maximum ductility of 5.9 (Table 2).

Specimens FWSCT-3 and FWSCT-5 under an axial load of 1967 kN ($\approx 0.2P_n$) reach a displacement ductility of 10.4 and 8, respectively. Ductility of Specimen FWSCT-5 is lower than that of Specimen FWSCT-3 because Specimen FWSCT-5 has larger number of fractured reinforcement than Specimen FWSCT-3. Specimen FWSCT-8 under a large axial load can reach a displacement ductility of 10.6. Figure 5 shows the curvature distribution along the column height, which is large at the top and bottom un-wrapped column ends (approximately 30 mm from the footing face). Except for both ends of the column, the curvature along the column height was about zero.

Figure 6 shows the comparison of normalized envelopes of five specimens after removing the P-Delta effect from the response curves. All specimens have similar initial stiffness, but Specimen FWSCT-0 shows significant strength reduction after reaching the maximum lateral force. The lateral force of columns is maintained in large drifts by using the FWSCT. The fact of increasing ductility with the increase of GFRP layers is not clear because longitudinal reinforcement fractures in the tests among Specimens FWSCT-3, FWSCT-5 and FWSCT-8.

5. ANALYTICAL RESULTS

Figure 7 shows the analytical results of Specimens FWSCT-1 and 3, where the test envelope was obtained after removing P-delta effects. The analytical curves calculated based on a constant plastic hinge length of 280 mm ($= gap + 0.022 f_{sy} d_b$) correlate well with the test responses. The residual shear strength curve (Figure 7(a)) intersects with the analytical curve at 3% drift, indicating shear failure as seen in the test of Specimen FWSCT-1. Figure 7(b) shows that the residual shear strength curve does not intersect

with the force-displacement curve of Specimen FWSCT-3, indicating no shear failure of FWSCT columns confined by more than 3 GFRP layers. However, the ACI 440 (2008) predicts shear failure in Specimens FWSCT-1 and FWSCT-3; the predicted shear strength is significantly underestimated.

Figure 8 plots shear forces of each component for Specimens FWSCT-1 and FWSCT-3. In small drift levels, the shear force is mainly carried by un-cracked concrete, V_c, and a compression strut mechanism of the applied axial load, V_p. A significant increase in shear resistance of the FRP jacket, V_{frp}, and the spiral corrugated tube, V_{sct}, starts from 2% drift. Specimen FWSCT-1 fails at 4% drift, where the shear resistance of the FRP jacket and the spiral corrugated tube are 20% and 13%, respectively. For Specimen FWSCT-3, the spiral corrugated tube yields at 4% drift, where the shear resistance of the FRP jacket and the spiral corrugated tube are 15%. The shear resistance of the FRP jacket can be 361 kN (32% of lateral force) at 7% drift.

6. CONCLUSIONS

Five large-scale reinforced concrete columns were tested to study the effects of the FRP-Wrapped Spiral Corrugated Tube (FWSCT) on the flexural and shear strengths in Taiwan. Test results showed that Specimen FWSCT-0 experienced shear failure at 1% drift and Specimen FWSCT-1 showed ductile-shear failure at 4% drift. Specimens FWSCT-3, FWSCT-5 and FWSCT-8 failed at 7~8% drift due to flexural rupture of longitudinal reinforcement. The following conclusions are drawn based on this study.

1. Test results indicated that the transverse reinforcement can be replaced by the FWSCT. The use of FWSCT significantly improves the seismic performance of concrete columns, increasing the ductility, energy dissipation and shear capacity. Although Specimen FWSCT-8 is under a constant high axial load level ($0.65P_n$ = 6856 kN), failure of longitudinal reinforcement starts at a displacement ductility of 10.6.
2. The FWSCT restraints the development of flexural and shear cracks in inner concrete core, so that the plastic hinge is limited to the unwrapped region (30 mm between the FWSCT and the footing face) plus the yield penetration length of longitudinal reinforcement in the footing. The proposed plastic hinge length is able to predict the lateral force and displacement relationship of FWSCT columns.
3. The failure strain, ε_{fu} of GFRP coupons are 1.9 ~ 2.5%. The strain when Specimen FWSCT-1 has fiber rupture in certain location is 0.9% because of distortion of fibers. The maximum FRP failure strain in other location is as high as 1.8% ($0.72\varepsilon_{fu}$). At 4% drift, the shear resistance of GFRP jacket in Specimens FWSCT-1 and FWSCT-3 are 198 kN (20% of lateral force) and 162 kN (15% of lateral force), respectively. The shear resistance of three GFRP layers in Specimen FWSCT-3 can be 361 kN (32% of lateral force) at 7% drift due to adequate shear strength.
4.

ACKNOWLEDGEMENTS

This work was funded by the National Science and Technology Center for Disaster Reduction (NCDR) under Program No. MOST 103-2119-M-002-010, Taiwan. The experimental work was conducted at the National Center for Research on Earthquake Engineering (NCREE) in Taiwan. Assistance from the technical staff is acknowledged.

REFERENCES

1. ACI 440 (2008). Guide for the design and construction of externally bonded FRP systems for strengthening concrete structure. Reported by ACI Committee.
2. Chou C-C, Lee C-S, Tan H-H, Wu K-Y (2014). “FRP Composite Wrapped Grooved-Wall Lining Tubular Structure, and Method of Manufacturing.” U.S. Patent No. US9566748 B2.
3. Chin V-L (2016). “Shear Strength Design and Tests of Circular Reinforced Concrete Columns Confined with a FRP-Wrapped Spiral Corrugated Tube.” Master Thesis, Advisor Chou C-C and Lee C-S, Department of Civil Engineering, National Taiwan University, Taiwan.
4. Gould N. C., and Harmon T. G. (2002). “Confined Concrete Columns Subjected to Axial Load, Cyclic Shear, and Cyclic Flexure—Part II: Experimental Program”, *ACI Structural Journal*, 99(1), pp. 42-50.
5. Kowalsky M. J., and Priestley M. J. N., “Improved Analytical Model for Shear Strength Circular Reinforced Concrete Columns in Seismic Regions,” *ACI Structural Journal*, Vol. 97, No. 3, May-June 2000, pp. 388-396.
6. Lee C-S and Hegemier G. A. (2009). Model of FRP-confined concrete cylinders in axial compression. *Journal of Composites for Construction*, 13(5), 442-454.
7. Lee C-S (2006). Modeling of FRP-jacketed RC columns subject to combined axial and lateral loads. University of California, San Diego.
8. Mirmiran A., Shahawy M., Samaan M., Echary H. E., Mastrapa J. C., & Pico O. (1998). Effect of column parameters on FRP-confined concrete. *Journal of Composites for Construction*, *2*(4), 175-185.
9. Pantazopolou S.J., and Mills R.H., “Microstructural Aspects of the Mechanical Response of Plain Concrete,” *ACI Materials Journal*, Vol. 92, No. 6, November-December 1995, pp. 605-616
10. Priestley M. J. N. and Seible F. (1991). ‘‘Seismic assessment and retrofit of bridges.’’ *Structural systems research project, Rep. No. SSRP-91/ 03*, M. J. N. Priestley and F. Seible, University of California, San Diego, Calif.
11. Priestley M. N., Seible F., Calvi G. M. (1996). *Seismic design and retrofit of bridges*. John Wiley & Sons.
12. Seible, F., Burgueño R., Abdallah M. G., & Nuismer R. (1996). Development of advanced composite carbon shell systems for concrete columns in seismic zones. In *Proc., 11th World Conf. Earthquake Engineering*. Oxford, UK: Pergamon, Elsevier Science.
13. Teng J.G., Yu T., Wong Y. L., Dong S.L. (2007). Hybrid FRP-concrete-steel tubular columns. *Construction and Building Material*, 21(4), 846-854.
14. Wu K-Y. (2015). “Seismic Tests of Circular Reinforced Concrete Columns Confined with a Spiral Corrugated Tube and Glass Fiber Reinforced Polymer (GFRP) Materials.” Master Thesis, Advisor Chou C-C and Lee C-S, Department of Civil Engineering, National Taiwan University, Taiwan. (in Chinese)
15. Xiao Y., Martin G. R., Yin Z., and Ma R. (1996). ‘‘Seismic retrofit of existing reinforced concrete bridge columns using a prefabricated composite jacketing system.’’ *Proc., 1st Int. Conf. on Composite in Infrastruct.*, University of Arizona at Tucson, Tucson, Arizona, 903–916.

Table 1 Specimen matrix

Specimens	H/D	f_c' (MPa)	Longitudinal Steel		Confinement		Axial Load P (kN)
			ρ_l	f_y(MPa)	Type	t_{tube}(mm)	
P1 Column 1/3 scale	2.33	35	2.23%	420	Steel Hoop #4 @ 4 cm	N/A	N/A
FWSCT-0	2.33	40*	2.15%	490*	SCT	0.54	1967 (0.19P_n)
FWSCT-1	2.33	35*	2.15%	450*	SCT+1 GFRP layer	1.44	1967 (0.19P_n)
FWSCT-3	2.33	35*	2.15%	450*	SCT+3 GFRP layers	3.44	1967 (0.21P_n)
FWSCT-5	2.33	40*	2.15%	490*	SCT+5 GFRP layers	6.04	1967 (0.21P_n)
FWSCT-8	2.33	40*	2.15%	490*	SCT+8 GFRP layers	9.44	6856 (0.65P_n)

Note: $*$ obtained from material test results
$t_{tube} = t_s + t_f$

Table 2 Test results

Specimens	Δ_y (mm)	Δ_u (mm)	V_{yield} (kN)	Peak Force		Ultimate Force	
				Ductility	±Force (kN)	Ductility	±Force (kN)
FWSCT-0	19	28	833	1.12	+911	1.4	+729
				1	-857	N/A	N/A
FWSCT-1	13.5	80	851	4.4	+1066	5.9	+998
				3	-1027	5.9	-941
FWSCT-3	13.5	140	893	4.4	+1131	10.4	+1047
				4.4	-1113	-10.4	-998
FWSCT-5	15	120	854	4	+1132	8	+1084
				-4	-1174	-8	-1087
FWSCT-8	15	160	1351	4	+1689	10.6	+1200
				-4	-1610	-10.6	-1072

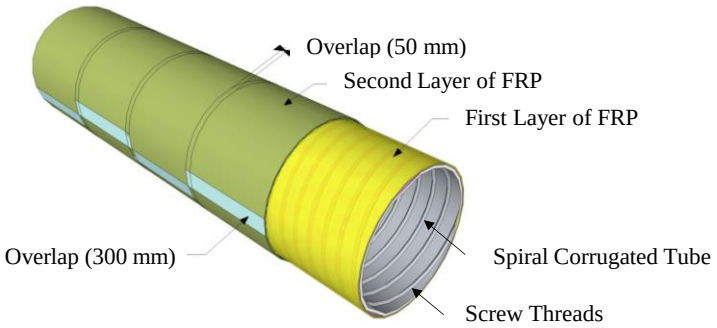

Figure 1 Schematic diagram of a GFRP-wrapped spiral corrugated tube

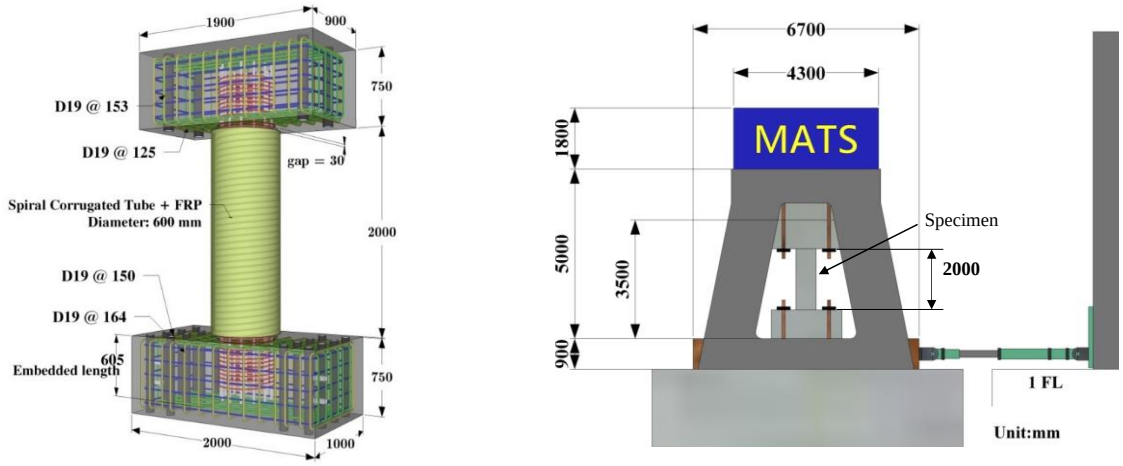

(a) Specimen FWSCT (b) Test setup

Figure 2 Specimen details and test setup

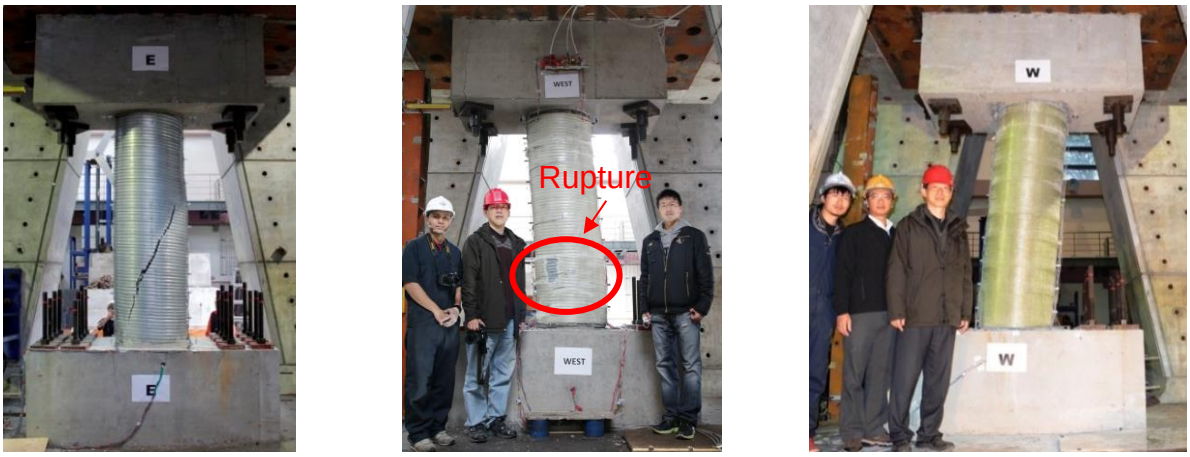

(a) Specimen FWSCT-0 (Drift = +1.4%) (b) Specimen FWSCT-1 (Drift = +6%) (c) Specimen FWSCT-8 (Drift = -8%)

Figure 3 Observations of specimens FWSCT-0, 1 and 8

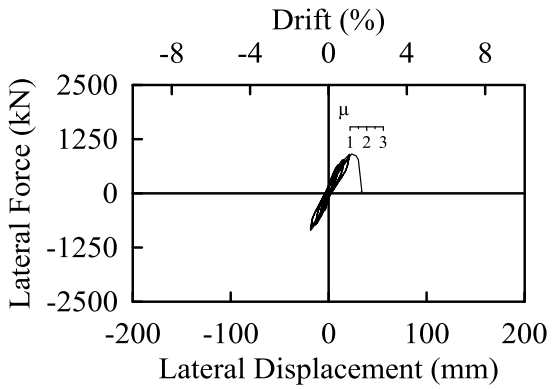

(a) Specimen FWSCT-0

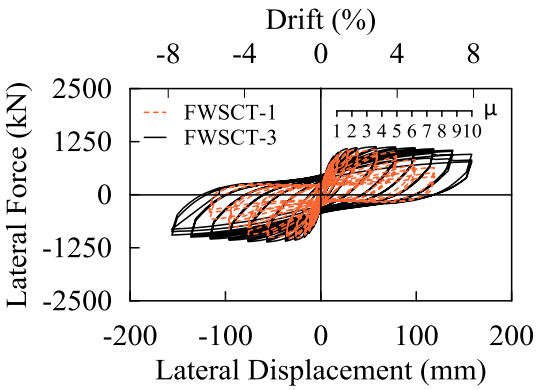

(b) Specimen FWSCT-1 and FWSCT-3

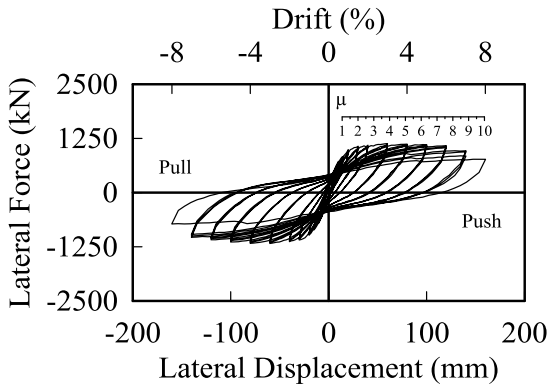

(c) Specimen FWSCT-5

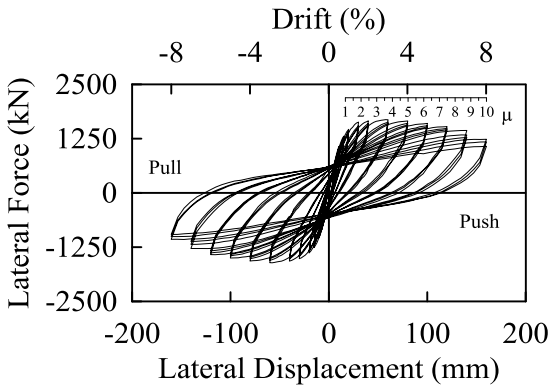

(d) Specimen FWSCT-8

Figure 4 Hysteretic loop of specimens FWSCT-0, 1, 3, 5 and 8

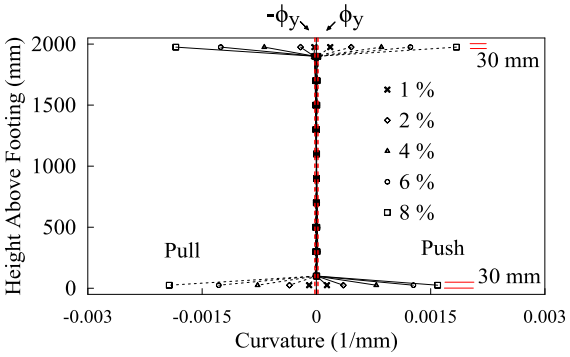

(a) Specimen FWSCT-3

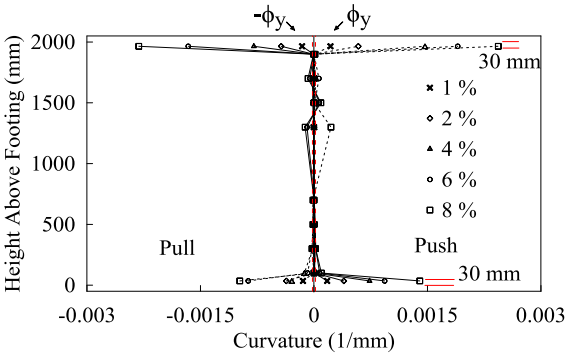

(b) Specimen FWSCT-8

Figure 5 Curvature of specimens FWSCT-3 and 8 from NDI along the column

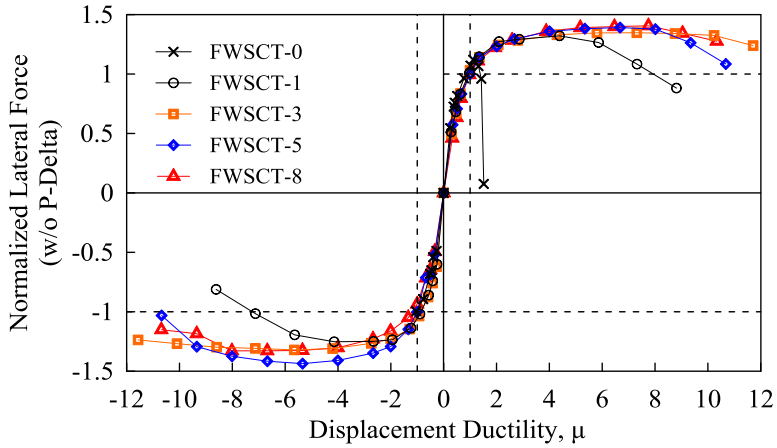

Figure 6 Normalized envelopes of specimens without P-Delta effect

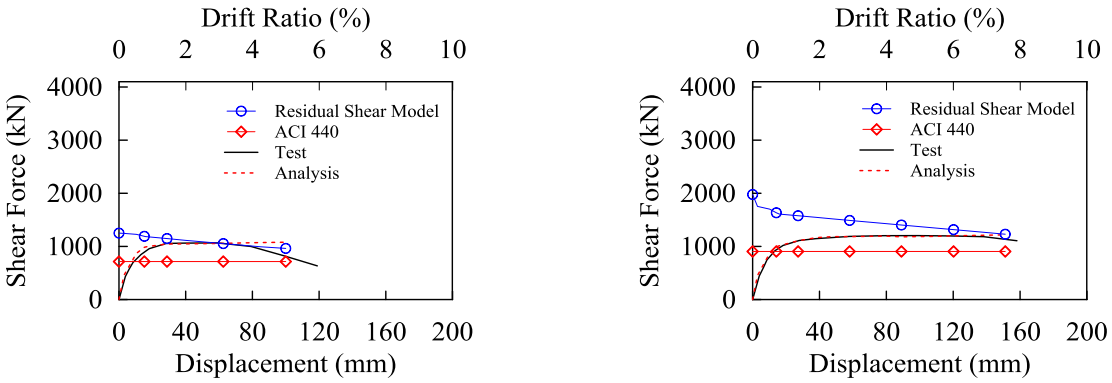

(a) Specimen FWSCT-1 (b) Specimen FWSCT-3

Figure 7 Comparison between analysis and test of specimens FWSCT-1 and 3

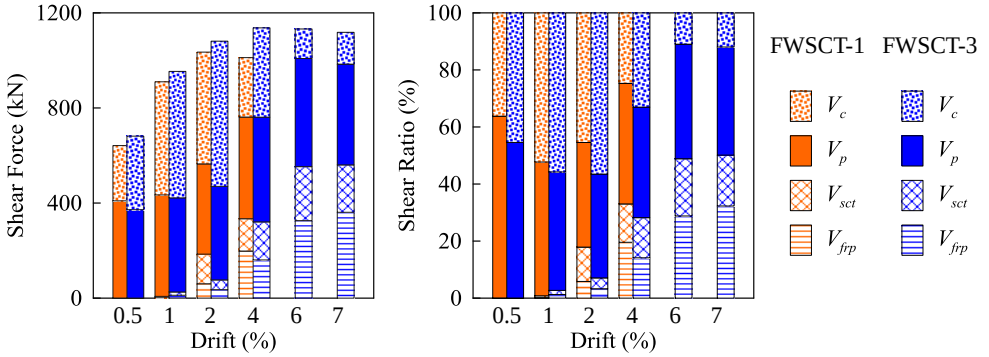

(a) Shear force (b) Shear force ratio

Figure 8 Shear force component in specimens FWSCT-1 and FWSCT-3